> REPLACE THIS LINE WITH YOUR MANUSCRIPT ID NUMBER (DOUBLE-CLICK HERE TO EDIT) <

Dimmable Optical Camera Communications with WDM Using RGB and Infrared LEDs

Hai Huang, Xiaodi You, Jin Shi, Jian Chen, Changyuan Yu, Senior Member, IEEE, Mingyi Gao, Senior Member, IEEE, and Gangxiang Shen, Senior Member, IEEE

Abstract—We propose an optical camera communication (OCC) system with dimming control, employing wavelength division multiplexing (WDM) with RGB and infrared (IR) light sources. The system uses pulse width modulation (PWM) for brightness adjustment, with IR transmission integrated into both PWM "ON" and "OFF" slots to compensate for data rate losses caused by dimming. To eliminate interference at the receiver, we implement a scheme that utilizes color correction and principal component analysis to separate the hybrid signal, with an optimization approach to fine-tune the IR intensity. This design achieves a data rate of 10.8 Kb/s at 30 fps under full dimming, offering a 33.3% improvement over RGB-only transmission. At a duty cycle of 0.5, the data rate further improves by 75.6%.

Index Terms—Optical camera communication (OCC), dimming control, wavelength division multiplexing (WDM).

I. INTRODUCTION

PTICAL camera communication (OCC), based on the rolling shuttle effect (RSE), is a branch of visible light communication (VLC) that provides a low-cost and convenient solution for integrated lighting and data transmission [1]. To accommodate varying lighting needs and promote energy efficiency [2], it is necessary to adjust lighting intensity, making dimming control essential in OCC systems. While many studies on dimming control have focused on photodetector (PD) receivers, few have explored its application with camera receivers [3], [4]. In [4], data was embedded within "ON" slots of commonly used pulse width modulation (PWM), with experiments confirming the feasibility of dimming in OCC systems. However, the frame rate of complementary-metaloxide-semiconductor (CMOS) cameras, typically ranging from 30 to 120 fps, often limits data rates of OCC significantly. Current approaches to increase data rates primarily involve enhanced modulation formats [5], as well as the use of RGB or multi-color light-emitting diodes (LEDs) for color shift keying (CSK) modulation [6] or wavelength division multiplexing (WDM) [7], [8]. By utilizing optical filters, OCC systems can expand beyond three WDM channels [9].

This paragraph of the first footnote will contain the date on which you submitted your paper for review, which is populated by IEEE.

This work was supported in part by National Natural Science Foundation of China (62001319), in part by Open Fund of IPOC (BUPT) (IPOC2020A009), and in part by HK RGC GRF (15212720). (Corresponding author: Xiaodi You)

Hai Huang, Xiaodi You, Mingyi Gao, and Gangxiang Shen are with School of Electronic and Information Engineering, Soochow University, Suzhou, Jiangsu 215006, China (e-mail: 20225228018@stu.suda.edu.cn; xdyou@suda.edu.cn; mygao@suda.edu.cn; shengx@suda.edu.cn).

Additionally, dimming control in VLC systems, particularly when using PWM, tends to reduce data rates due to its strong dependence on the duty cycle. This effect is also observed in OCC systems, whether using a single light source [4] or multiple sources with WDM. To boost data rates, PD-based VLC systems can leverage infrared (IR) signals either as an additional wavelength for WDM [10] or to fill PWM "OFF" slots during dimming [11], thereby increasing the overall data rate. IR transmission has also proven to work effectively in OCC systems [12]. However, in OCC systems with dimming control, the use of WDM with IR has been little investigated.

In this paper, we propose an OCC system with dimming control that utilizes four-channel WDM with RGB and IR, integrating IR into the entire transmission process while applying PWM for full-range dimming of RGB channels. To address the interference introduced by IR on RGB components, we present a scheme to eliminate IR interference and accurately extract the hybrid signals at the receiver without the use of optical filters. Additionally, a wavelet decomposition-based approach is implemented to optimize IR signal strength. Experimental results show the effectiveness of the proposed system, achieving stable transmission across various dimming levels from 1 to 0, with bit error rates (BERs) ranging from 5.0 $\times 10^{-2}$ to 1.6×10^{-3} , and data rates from 10.8 Kb/s to 3.3 Kb/s.

II. PROPOSED OCC SYSTEM

A. Transmitter Design

Figure 1 shows the schematic diagram of the proposed OCC system with WDM, consisting of four channels: RGB and IR. PWM is used to control the brightness, with RGB and IR LEDs modulated using on-off-keying (OOK). The hybrid signals are then emitted. A CMOS camera serves as the receiver, using the RSE to capture the received signal as a series of stripes. Example frame images obtained at different stages of the system are shown in Figs. 1(a)~(e). Fig. 2 illustrates the transmitted frame structure, where each frame contains two repeated packets to ensure the camera captures at least one

Jin Shi is with School of Information Engineering, Wuhan University of Technology, Wuhan 430070, China (e-mail: jinshi@whut.edu.cn).

Jian Chen is with School of Telecommunications and Information Engineering, Nanjing University of Posts and Telecommunications, Nanjing 210003, China (e-mail: chenjian@njupt.edu.cn).

Changyuan Yu is with Photonics Research Institute, Department of Electrical and Electronic Engineering, Hong Kong Polytechnic University, Hung Hom, Hong Kong (e-mail: changyuan.yu@polyu.edu.hk).

Color versions of one or more of the figures in this article are available online at http://ieeexplore.ieee.org

© 2025 IEEE. Personal use of this material is permitted. Permission from IEEE must be obtained for all other uses, in any current or future media, including reprinting/republishing this material for advertising or promotional purposes, creating new collective works, for resale or redistribution to servers or lists, or reuse of any copyrighted component of this work in other works.

Fig. 1. Block diagram of the proposed system, and corresponding frame images: (a) frame image before segmentation; (b) hybrid WDM frame image during "ON" slots; (c) IR-only frame image during "OFF" slots; (d) color-corrected version of (b); and (e) preprocessed image for PCA during "ON" slots.

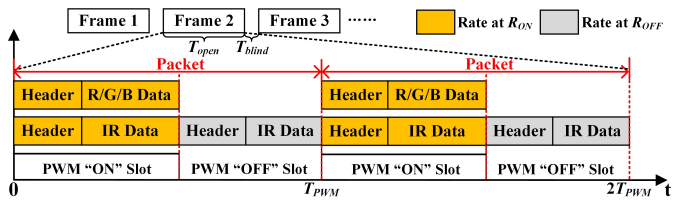


Fig. 2. Frame structure of the proposed system.

complete packet per frame image, preventing data loss during the camera's blind time. Each packet is transmitted across PWM "ON" and "OFF" slots. During "ON" slots, four subpackets in the RGB and IR channels are transmitted in parallel at the same lower speed to ensure clear frame capture by the camera. During "OFF" slots, only the invisible IR sub-packet is transmitted at a higher speed to improve spectral efficiency. This approach ensures that the continuous IR transmission compensates for data rate losses due to dimming. Based on the camera parameters, the PWM period is calculated as follows:

$$T_{PWM} \square T_{open} / [2 \cdot (T_{open} \square T_{blind}) \cdot F], \tag{1}$$

where T_{open} and T_{blind} represent the time within a frame that information can be read and the blind time, respectively, both determined by the camera, and F is the frame rate. The symbol rates of the sub-packets during "ON" (R_{ON}) and "OFF" (R_{OFF}) slots of PWM are derived as:

$$Ron / off \square Lon / off / T_{PWM},$$
 (2)

where $L_{ON/OFF}$ is the equivalent sub-packet length (in symbols) when it occupies the full PWM period. By selecting appropriate values of L_{ON} and L_{OFF} , R_{ON} and R_{OFF} are determined to balance transmission quality and efficiency. When the PWM duty cycle D changes, both R_{ON} and R_{OFF} remain constant. However, the sub-packet lengths during PWM "ON" (l_{ON}) and "OFF" (l_{OFF}) slots need to be adjusted based on D and can be derived by:

$$\begin{cases} lo_N \square Ro_N \cdot T_{PWM} \cdot D \\ lo_{FF} \square Ro_{FF} \cdot T_{PWM} \cdot (1-D) \end{cases}$$
(3)

Accordingly, the system data rate is calculated as:

$$C \square [4 \cdot D \cdot SEon \cdot Lon \square (1-D) \cdot SEoff \cdot Loff] \cdot F,$$
 (4)

where $SE_{ON/OFF}$ is the spectral efficiency per channel during "ON" or "OFF" slots, respectively (1 bit/symbol for OOK).

B. Receiver Design

At the receiver, a complete PWM period is identified in each frame image based on the frame header, followed by dimming recognition to distinguish between "ON" and "OFF" slots. This is achieved by leveraging the significant difference in the G-channel grayscale values between the four-channel hybrid signal and the pure IR signal. To enhance this difference, the row grayscale values are squared to generate a signal energy

curve. The starting point of the "ON" slot is identified as the pixel where the slope changes abruptly, and the grayscale values consistently rise, exceeding half of the maximum value.

Next, we extract RGB signals during "ON" slots. However, RGB signals are affected by the IR component. To reduce this influence, the hybrid signal image is converted to the YCrCb format, and a color correction value is calculated by [13]:

$$y_{\Delta} \square \Sigma_{n \square}^{N} \Sigma_{m \square}^{M} y_{n,m} \mathsf{T} \sqrt{\frac{\sum_{n \square}^{N} \Sigma_{m \square}^{M} [y_{n,m} \mathsf{T} (\Sigma_{n \square}^{N} \Sigma_{m \square}^{M} y_{n,m} / NM)]^{2}}{NM}}$$
(5)

Here, $y_{n,m}$ denotes the Cb/Cr channel value of all pixels, while N and M are the number of rows and columns of the frame image, respectively. We subtract y_{Δ} from the Cb/Cr channel values of the original frame image and apply a Gaussian filter to smooth the image. Finally, the image is converted back to the RGB format, with IR components effectively removed.

We then extract the IR signal during "ON" slots. First, the hybrid frame image is converted to the HSV format, and a mean filter is applied to reduce noise while enhancing the hue and saturation. Then, the image is converted back to the RGB format. Since the IR signal affects all three RGB channels, we use principal component analysis (PCA), an effective technique for linear dimensionality reduction, to extract common features across these channels [8]. By applying PCA, we can effectively separate the IR component from the hybrid signal. The process begins by calculating the covariance matrix [8]:

$$\mathbf{V} \square \mathbf{X_c}^{\mathsf{T}} \mathbf{X_c} / \square \mathbf{s} - 1 \square \square (\mathbf{X} - \mathbf{A} \boldsymbol{\mu}^{\mathsf{T}})^{\mathsf{T}} (\mathbf{X} - \mathbf{A} \boldsymbol{\mu}^{\mathsf{T}}) / \square \mathbf{s} - 1 \square, (6)$$

where X is the grayscale value matrix of the RGB channels, A is a matrix of ones, μ is the mean vector for each channel, X_c is the de-centered matrix, and s is the number of samples. Next, eigenvalue decomposition is performed on V, and the top h eigenvectors in descending order are selected to form the matrix V_h . Finally, the de-centered data is projected into the principal component space to obtain the reduced data matrix $Y = X_c V_h$, where the first component of Y represents the IR signal.

For "OFF" slots, which contain only IR components, PCA is directly applied to extract the IR signal.

C. IR Intensity Optimization

Since the received signal contains both RGB and IR, higher IR intensity can interfere with RGB signals, complicating demodulation, while lower IR intensity reduces extraction accuracy. To optimize IR intensity, we use wavelet decomposition to separate the signal into multiple scales and frequencies (Eq. (2.52) in [14]). The R-channel grayscale values, primarily affected by the IR signal, are used for analysis. To intuitively obtain the energy distribution, the energy of the wavelet-decomposed signal at level *j* can be defined as:

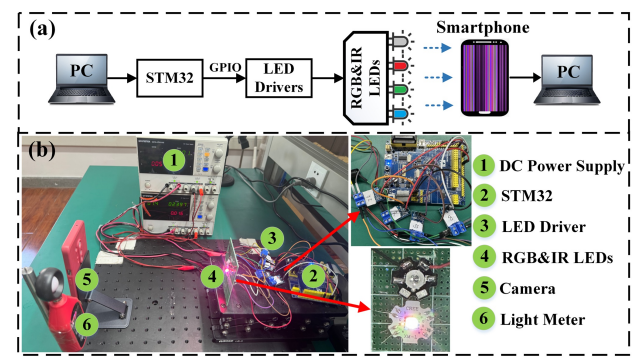


Fig. 3. Experimental setup: (a) schematic diagram; and (b) photographs.

$\label{table I} TABLE\ I$ Sub-packet Lengths Adopted for Various Dimming Levels

$L_{ON} = 40$											
D	0	0.1	0.2	0.3	0.4	0.5	0.6	0.7	0.8	0.9	1
l_{ON}	0	4	8	12	16	20	24	28	32	36	40
l_{OFF}	110	99	88	77	66	55	44	33	22	11	0
$L_{ON} = 90$											
D	0	0.1	0.2	0.3	0.4	0.5	0.6	0.7	0.8	0.9	1
l_{ON}	0	9	18	27	36	45	54	63	72	81	90
l_{OFF}	110	99	88	77	66	55	44	33	22	11	0

$$E_{j} = \begin{cases} \sum_{k = 1}^{N_{a}} a_{J,k}^{2}, & j = J \\ \sum_{k = 1}^{N_{d}} d_{j,k}^{2}, & j = 1, 2, \dots, J - 1, \end{cases}$$

$$(7)$$

where j is the scale index, k is the position index, J is the number of decomposition levels, $a_{J,k}$ is the approximation coefficient, $d_{j,k}$ is the detail coefficient, N_a is the number of approximation coefficients at level J, and N_d is the number of detail coefficients at level j [14]. We perform linear fitting on the largest calculated energy values to minimize the influence of noise and non-dominant signals, thereby emphasizing the key signal characteristics. The slope of the fitted line, determined using the least squares method [13], quantifies the impact of IR intensity on the R-channel. A larger slope indicates an energy imbalance, while a smaller slope suggests a more balanced distribution. The voltage corresponding to the smallest slope is selected as the optimal input for the IR LED driver.

III. EXPERIMENTAL RESULTS AND DISCUSSIONS

Figure 3 shows the experimental setup. We test various PWM duty cycles from 1 to 0 in 0.1 intervals. For each duty cycle, original data generated by a personal computer (PC) is used to construct sub-packets, which are then sent to an STM32 microcontroller (ALIENTEK MiniSTM2F103). This signal is loaded into four LED drivers connected to RGB LEDs (CREE XM-L RGBW) and an IR LED (FANGPU FOVNNSTF3W-940NM). The input voltages for the RGB LEDs are regulated between 3V and 3.7V, producing white light with a color rendering index (CRI) of ~80. The signal passes through 20 cm of free space and is captured by a CMOS camera from a smartphone (OnePlus 8 Pro, rear main camera) that records it as a video. The camera is set with a resolution of 1920×1080, an exposure time of 1/15360 s, an ISO of 6400, and a frame rate of 30 fps. To enable IR detection and reduce blooming effect, we physically remove the camera's IR filter [12] and place a general translucent white oil paper in front [5]. The video is processed on a PC for demodulation using MATLAB. A light

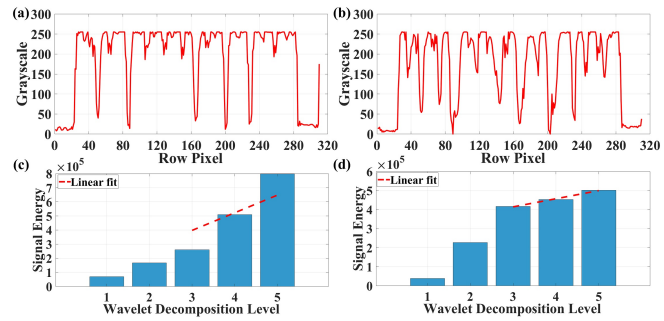


Fig. 4. R-channel grayscale values with IR LED driver input voltage set at: (a) 1.8 V (w/o optimization); (b) 1.3 V (w/o optimization). Calculated signal energy: (c) corresponding to (a); and (d) corresponding to (b). ($L_{ON} = 40$)

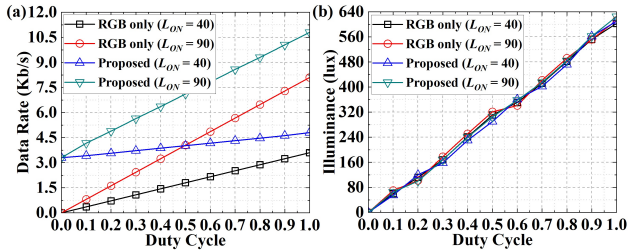


Fig. 5. (a) Data rates; and (b) illuminance measured at various dimming levels. meter (UNI-T UT383) placed near the camera measures light intensity. During "ON" slots, two equivalent sub-packet lengths are tested: $L_{ON} = 40$ and $L_{ON} = 90$, to evaluate the BER and data rate. Using Eq. (4), this results in a maximum data rate of $4 \times 1 \times 90 \times 30 = 10.8$ Kb/s at full dimming. During "OFF" slots, we fix L_{OFF} at 110 to maximize spectral efficiency. Table I lists the sub-packet lengths for various dimming levels, as optimized by Eq. (3). Each sub-packet includes a 5-bit header, except for D = 0.1 and $l_{ON} = 4$, where a 3-bit header is used.

We first analyze the influence of IR on RGB signals. Fig. 4 shows an example of the R-channel grayscale values at different IR LED driver input voltages, along with the corresponding signal energy, at $L_{ON} = 40$ and a duty cycle of 1. As in Fig. 4(a), when the voltage is set to its maximum rated value of 1.8V, the R-channel grayscale waveform exhibits saturation due to the influence of IR. Using the DB4 wavelet function, the signal is decomposed into five levels, and the energy of each level is calculated, as shown in Fig. 4(c). The top three energy values are selected for linear fitting, resulting in a slope of 1.25×10^5 . To optimize the IR intensity, different voltage levels are tested with a resolution of 0.1V. It is observed that at 1.3V, the fitted line has the smallest slope of 0.43×10^5 , as shown in Fig. 4(d). Under this condition, the R-channel signal retains its overall waveform without significant distortion, as in Fig. 4(b). For Lon = 90, the optimal value is also 1.3V. Therefore, 1.3V is fed into the IR LED driver in subsequent experiments.

Figure 5 illustrates the measured data rates and illuminance at varying dimming levels for $L_{ON}=40$ and $L_{ON}=90$. For comparison, we include the RGB-only scheme, which shares the same modulation, sub-packet lengths, and data rate per wavelength as the proposed scheme. In Fig. 5(a), when D=0, the RGB-only scheme fails to establish communication, whereas the proposed scheme achieves basic communication at 3.3 Kb/s via the IR channel. As the dimming level increases, the data rates for both schemes improve. For example, with $L_{ON}=90$, at dimming levels of 0.3, 0.5 and 1, the RGB-only scheme

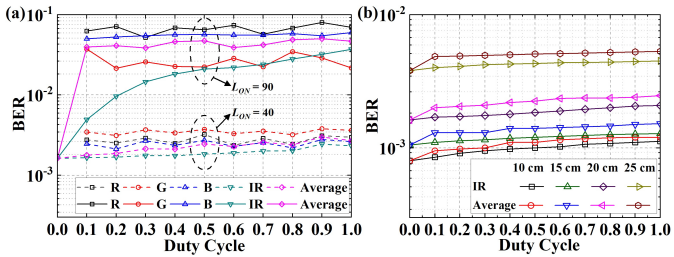


Fig. 6. BERs under different D with changes in: (a) L_{ON} ; and (b) distances.

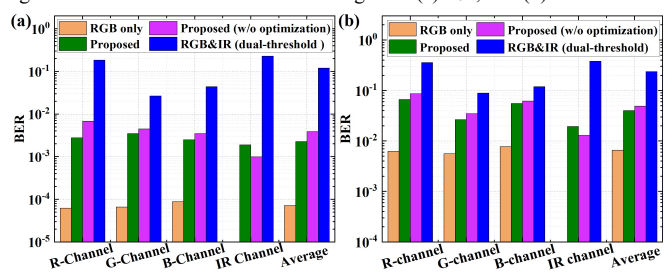


Fig. 7. Average BERs of different schemes: (a) $L_{ON} = 40$; and (b) $L_{ON} = 90$.

achieves data rates of 2.43 Kb/s, 4.05 Kb/s and 8.1 Kb/s, respectively. In contrast, the proposed scheme enhances these rates to 5.64 Kb/s, 7.11 Kb/s, and 10.8 Kb/s, corresponding to improvements of 132.1%, 75.6%, and 33.3%. A similar trend is observed for $L_{ON} = 40$, with the improvement being more pronounced due to the relatively higher contribution of the IR channel. Fig. 5(b) demonstrates that both schemes exhibit a nearly linear increase in illuminance as the dimming level rises.

Figure 6(a) compares the BERs of the proposed scheme at varying dimming levels with different sub-packet lengths. For $L_{ON} = 90$, the average BER ranges from 5.0×10^{-2} to 1.6×10^{-3} as the duty cycle decreases from 1 to 0. Specifically, the BER of RGB channels remains at the 10⁻² level, while the BER of IR channel improves from 3.7×10^{-2} to 1.6×10^{-3} . This is because, as the dimming level decreases, RGB signals introduce less interference, enhancing the IR channel's BER performance. For $L_{ON} = 40$, a similar trend is observed, with the average BER ranging from 2.9×10^{-3} to 1.6×10^{-3} . Additionally, as L_{ON} increases, the received stripes become ambiguous, leading to higher BERs across all channels and significantly degrading transmission quality. Fig. 6(b) compares the BERs at different propagation distances ranging from 10 cm to 25 cm at $L_{ON} = 40$. Results show that as the distance increases, both the BER of IR and average BER rise. This can be attributed to the decreasing signal-to-noise ratio, which also leads to ambiguous stripes.

Figure 7 compares average BERs of each channel across all dimming levels for several schemes: the RGB-only scheme, the proposed scheme with and without IR intensity optimization, and the dual-threshold scheme. The dual-threshold scheme first treats the IR signal as noise and applies dual thresholds to identify high and low levels of RGB signals. It then extracts the IR signal by subtracting the extracted RGB signals from the hybrid signal. In Fig. 7(a), the RGB-only scheme achieves the best BER, but at the cost of significantly reduced data rates. The proposed scheme slightly increases the average BER compared to the RGB-only scheme but remains a value below 2.3 × 10⁻³, demonstrating an improvement over both the scheme without IR intensity optimization and the dual-threshold scheme. Fig.

7(b) shows a similar trend for $L_{ON} = 90$, confirming that the proposed scheme effectively balances BER and data rate.

IV. CONCLUSION

We proposed a dimmable single-camera OCC system based on PWM and four-channel WDM, incorporating an IR channel with RGB channels while eliminating signal interference without optical filters. Experimental results showed that, at L_{ON} = 40, the system achieved stable BERs in the 10^{-3} range across various dimming levels. At L_{ON} = 90, the data rate reached 10.8 Kb/s under full dimming. Furthermore, data rates improved by 33.3%, 75.6%, and 132.1% at dimming levels of 1, 0.5 and 0.3, respectively, compared to RGB-only systems. Across the full dimming range from 1 to 0, the system maintained stable data rates no lower than 3.3 Kb/s and BERs below 5.0×10^{-2} . Our future work will involve the use of advanced image sensors and higher frame rates to achieve enhanced data rates.

REFERENCES

- [1] N. Saha, M. S. Ifthekhar, N. T. Le, and Y. M. Jang, "Survey on optical camera communications: challenges and opportunities," *IET Optoelectronics*, vol. 9, no. 5, pp. 172–183, Oct. 2015.
- [2] K. Lee and H. Park, "Modulations for visible light communications with dimming control," *IEEE Photonics Technology Letters*, vol. 23, no. 16, pp. 1136–1138, Aug. 2011.
- [3] Q. Wang, P. Zhang, Y. Sun, and Y. Yang, "A general model for dimmable optical camera communication," in Proc. International Conference on Sensing, Measurement & Data Analytics in the era of Artificial Intelligence (ICSMD), pp. 1–7, Oct. 2021.
- [4] H. Huang, X. You, J. Shi, J. Chen, C. Yu, M. Gao, and G. Shen, "Experimental demonstration of optical camera communications supporting dimming control," in *Proc. OptoElectronics and Communications Conference (OECC)*, pp. 1–3, Jul. 2023.
- [5] J. Shi, J. He, Z. Jiang, and G. -K. Chang, "Modulation format shifting scheme for optical camera communication," *IEEE Photonics Technology Letters*, vol. 32, no. 18, pp. 1167–1170, Sep. 2020.
- [6] H. -W. Chen et al., "Color-shift keying for optical camera communication using a rolling shutter mode," *IEEE Photonics Journal*, vol. 11, no. 2, pp. 1–8, Apr. 2019, Art. no. 7901808.
- [7] P. Luo *et al.*, "Experimental demonstration of RGB LED-based optical camera communications," *IEEE Photonics Journal*, vol. 7, no. 5, pp. 1–12, Oct. 2015, Art. no. 7904212.
- [8] M. De Murcia, H. Boeglen, A. Julien-Vergonjanne, and P. Combeau, "Principal component analysis for robust region-of-interest detection in NLOS optical camera communication," in *Proc. International Symposium* on Communication Systems, Networks and Digital Signal Processing (CSNDSP), pp. 383–388, Jul. 2024.
- [9] H. Chen et al., "Quadrichromatic LED based mobile phone camera visible light communication," Optics Express, vol. 26, no. 13, pp. 17132–17144, Jun. 2018.
- [10] C. Lee et al., "26 Gbit/s LiFi system with laser-based white light transmitter," Journal of Lightwave Technology, vol. 40, no. 5, pp. 1432– 1439, Mar. 2022.
- [11] S. Liu, X. You, J. Chen, C. Yu, C. Xiong, M. Gao, and G. Shen, "Real-time implementation of hybrid visible light/infrared communications supporting full-range dynamic dimming control," *IEEE Photonics Journal*, vol. 16, no. 1, pp. 1–14, Feb. 2024, Art. no. 7300514.
- [12] W. A. Cahyadi and Y. H. Chung, "Experimental demonstration of indoor uplink near-infrared LED camera communication," *Optics Express*, vol. 26, no. 15, pp. 19657–19664, Jul. 2018.
- [13] S. J. Miller, "The method of least squares," *Mathematics Department Brown University*, vol. 8, pp. 1–12, 2006.
- [14] I. Daubechies, "Orthonormal bases of compactly supported wavelets," Communications on Pure and Applied Mathematics, vol. 41, no.7, pp. 909–996, Oct. 1988.